Journal of Power Sources 219 (2012) 263–271

Contents lists available at SciVerse ScienceDirect

Journal of Power Sources

journal homepage: www.elsevier.com/locate/jpowsour

N-methyl-2-pyrrolidone as a solvent for the non-aqueous electrolyte of rechargeable Li-air batteries

Hui Wang*, Kai Xie, Lingyan Wang, Yu Han

Department of Material Engineering and Applied Chemistry, National University of Defense Technology, Changsha 410073, China

HIGHLIGHTS

- ► NMP shows increased chemical stability to superoxide radical.
- ► LiO_2 is instable and can decompose to Li_2O_2 in Li-containing NMP based electrolyte.
- ► Li_2O_2 can decompose at high potential and Au could catalyse this procedure.
- ► Cells with NMP based electrolytes shows good cyclic performance.
- ► Selection of binders is important to avoid decomposition of NMP on air electrode.

ARTICLE INFO

Article history:
Received 30 April 2012
Received in revised form
14 July 2012
Accepted 21 July 2012
Available online 27 July 2012

Keywords:
N-methyl-2-pyrrolidone
Lithium peroxide
Electrolytes stability
Cycle performance
Li-air battery

ABSTRACT

The instability of solvent molecules toward oxygen reduction species is the main reason for the performance deterioration of rechargeable Li-air batteries. Identifying the appropriate electrolyte solvents is one prerequisite for the application of Li-air batteries. In this article, we study *N*-methyl-2-pyrrodione (NMP) as a solvent for the non-aqueous electrolyte of Li-air batteries. Oxygen reduction reactions (ORRs) and oxygen oxidation reactions (OERs) are investigated on Au and glassy carbon (GC) electrodes in NMP-based terabutylammonium perchlorate ($TBAClO_4$) and lithium perchlorate ($LiClO_4$) electrolyte solutions using the cyclic voltammetry method. Raman and X-ray photoemission spectra (XPS) are used to detect the species on the electrode surface during cell cycles. The results show that while the one-electron O_2/O_2^- reversible couples are observed in $TBAClO_4$/NMP, in presence of Li ion, the initially formed LiO_2 generated by one-electron transfer process decomposes to Li_2O_2. As the predominant discharge products, Li_2O_2 decomposes during the recharge processes. The cells using NMP-based electrolytes exhibit good cycle performance, and the first cycle efficiency is approximately 97%. Although the decomposition of NMP occurs on the air electrode surface during the cells recharge, the increased chemical stability against oxygen reduction species offer NMP-based electrolytes as potential candidates for rechargeable Li-air batteries electrolytes.

1. Introduction

Among the currently available electrochemical energy storage systems, the aprotic electrolyte rechargeable Li-air batteries could provide the highest energy density; these batteries have a theoretical value of approximately 11,700 Wh kg^{-1}. With advantages of safety and simplicity, Li-air batteries based on non-aqueous could be the basic configuration for the future power system of hybrid electric vehicles (HEVs) and electric vehicles (EVs) [1–3]. However, before this promising technology becomes a reality, there are many scientific and technical challenges that must be overcome. One prerequisite for the development of Li-air batteries that have both high capacity and excellent cycle performance is the identification of a non-aqueous electrolyte that could maintain the physical and chemical properties and that is not significantly decomposed in the air cathode during cell operation [4].

During early studies on the electrolytes for Li-air batteries, organic carbonate solvents such as propylene carbonate (PC), ethylene carbonate (EC) and dimethyl carbonate (DEC), which are commonly used electrolytes in Li-ion batteries, were the main research focus. These studies focused on the properties of solvents that influence the oxygen transport properties, such as solubility and diffusion in electrolytes [5–8], whereas little attention was paid to the stability of the electrolytes during the discharge/charge process. However, recent studies have shown that during the discharge process, the products on the cathode in organic

* Corresponding author. Tel.: +86 731 84573149; fax: +86 731 84573150.
E-mail address: wanghuichn1234@gmail.com (H. Wang).

0378-7753/$ – see front matter © 2012 Elsevier B.V. All rights reserved.
http://dx.doi.org/10.1016/j.jpowsour.2012.07.065

carbonate electrolytes were not Li_2O_2 but various alkyl carbonates, such as Li_2CO_3, $C_3H_6(OCO_2Li)_2$, HCO_2Li and CH_3CO_2Li [9–12]. Many results have been obtained from Fourier transform infrared (FTIR) spectroscopy, Raman spectroscopy and X-ray diffraction (XRD) patterns, and these results have provided evidence of the formation of the above compounds. CO_2 is the predominant oxidation product that was detected by in-situ differential electrochemical mass spectrometry (DEMS), which also demonstrated that the decomposition during recharge was in fact the oxidation of lithium carbonate and other alkyl carbonate, not Li_2O_2 [13,14]. The instability of solvent molecules eventually results in the failure of batteries after a few cycles.

The superoxide anion radical ($O_2^{\bullet-}$) as the primary intermediate in aprotic media during the oxygen reduction process is believed to be the reason for the decomposition of the carbonate solvents. Bryantsev et al. demonstrated that the nucleophilic attack of $O_2^{\bullet-}$ at the ethereal carbons of carbonate is the most probable mechanism for the degradation of carbonate molecules through the use of density functional theory [9]. To identify solvents that were stable for the O_2 reduction species, many other electrolytes for lithium-air batteries have been investigated, especially ether-based electrolyes [14–17]. McCloskey et al. reported that Li_2O_2 was the main discharge product in the dimethoxyethane (DME)-based electrolyte and that the oxidation of solvents only occurred at sufficiently high charging voltage [14]. In contrast, the results reported by Freunberger et al. showed that electrolytes based on ether also exhibited decomposition during discharge [16]. In our previous published work, we also observed that ether molecules were instable for the $O_2^{\bullet-}$ because the ether formed peroxide after a long exposure to O_2 [18]. Zhang et al. introduced an oligoether-functionalised silane electrolyte. The increased stability of this solvent toward the oxygen reduction species was attributed to the ether functional group [19]. In addition to organic solvents, ionic liquids based electrolytes for lithium-air batteries have also been investigated. Kuboki et al. studied the performance of Li-O_2 batteries using an ionic liquid as the electrolyte in an ambient environment [20]. Allen et al. reported a highly reversible reduction on the Au electrode in a Li^+-containing room-temperature ionic liquid and observed that the gold surface is particularly beneficial for the oxidation reactions [21].

As one of the common organic solvents, *N*-methyl-2-pyrrolidone (NMP) has desirable properties such as low viscosity, low flammability and relatively low toxicity. Because NMP belongs to the class of dipolar aprotic solvents, it also has an appropriate high polarity and can dissolve most Li-salts, such as $LiClO_4$. Because of the above-mentioned properties, NMP is a potentially useful candidate for the electrolyte employed in Li-air batteries. Results from previous calculations have shown that NMP was stable in the presence of oxygen reduction species such as $O_2^{\bullet-}$ and $LiO_2^{\bullet}$ [4]; however, the actual performance of the batteries using NMP as electrolytes was not reported. In this article, we first identified the different oxygen reduction reactions (ORRs) and oxygen oxidation reactions (OERs) on gold (Au) and glassy carbon (GC) electrodes in NMP based electrolytes using cyclic voltammetry. We then examined the cyclic performance of Li-air cells using NMP as electrolytes and systematically studied the composition of the deposits that form on the air electrode surface during cycles. These results, combined with previous research findings, are expected to provide some guidelines for the selection of non-aqueous electrolytes for further development of Li-air batteries.

2. Experimental

2.1. Li-O_2 cell assembling and electrochemical test

The porous electrode was prepared by casting a slurry mixture of Super P carbon (TIMCAL Graphite & Carbon) and F105 binder (a water-based adhesive, purchased from Chengdu INDIGO Power Sources Co. Ltd.) with a weight ratio of 3:1 onto a nickel foam collector (Changsha Lyrun Material Co. Ltd.). The cathodes were dried at 120 °C for 2 h, and then dried overnight at 80 °C to completely remove the solvents. NMP-based electrolytes (0.1 M) were prepared by mixing *N*-methyl-2-pyrrolidone (Sigma–Aldrich, battery grade, $H_2O < 10$ ppm) with terabutylammonium perchlorate ($TBAClO_4$, electro-chemical grade > 99.0%, Chengdu Best Reagent Co. Ltd.) or lithium perchlorate ($LiClO_4$, battery grade > 99.9%, Sigma–Aldrich). The commercial electrolyte solution of 0.1 M $LiClO_4$/PC was purchased from Novolyte Technologies Co. Ltd. All of the chemicals were stored and prepared in a glove box, where the moisture and oxygen content was less than 1 ppm. The cyclic voltammetry experiments were performed using an Autolab (Ecochemie Inc., model-PGSTAT 30) potentiostat. The electrochemical cells consisted of a traditional three-electrode system utilizing platinum (Pt) foil as the counter electrodes and inlet/outlet valves for gas purging. Narrow Li foil was used directly as the reference electrode because Li/Li^+ has a stable standard potential (~ -3.40 V) in NMP [22]. Tests of the cycling performance were conducted using a Land cycler (Wuhan Land Electronic Co. Ltd.) within a voltage range from 2.0 V to 4.1 V (vs. Li^+/Li) at a current density of 0.1 mA cm^{-2} in the self-designed cells. The cells were constructed as reported in our previously published work. All of the above tests were conducted under pure O_2 and at room temperature (25 °C).

2.2. Characterization

The cycled cells were disassembled in an Ar-filled glove box. The cathodes were rinsed twice with DME and then dried under an Ar atmosphere. The Raman spectra of the cathodes were collected on a Bruker SENTERRA Raman spectrometer. For the Raman measurements, the excitation source is the 532 nm line from a Krypton laser with a power of 20 mW. X-ray photoemission spectroscopy (XPS) measurements were performed on a K-Alpha 1063 (Thermo Fisher Scientific) spectrometer with monochromatic Al-Kα used as the excitation source. During the XPS measurements, the typical analysis area was 400 μm in diameter, and the pressure in the analysis chamber is 10^{-9} mbar. The binding energy scale was corrected based on the C1s peak from contaminations (approximately 284.8 eV) and used as the internal binding energy standard. N_2 adsorption-desorption data was collected using a QuadraSorb SI (Quantachrome) automated gas sorption system. The total pore volume and pore distribution is evaluated by the Density Functional Theory (DFT) methods.

3. Results and discussion

The ORRs and OERs on the Au and GC electrodes are first studied in a $TBAClO_4$/NMP electrolyte. The cyclic voltammograms (CVs) in the $TBAClO_4$/NMP electrolyte at various scan rates on the Au and GC electrodes are shown in Fig. 1. As shown, both voltammograms exhibit a couple of reversible peaks in the scan range from 2.0 V to 4.0 V (vs. Li/Li^+); the reduction peak is at approximately 2.4 V, and there is little difference in the CVs from the Au and GC electrodes. The oxidation peak shape is quite similar to the reduction peak, and the position of the redox peaks is slightly separated in the $ClO_4^{\bullet}$ case [23]. By integrating the area under each peak, the anodic to cathodic area is approximately one. The inset graphs in Fig. 1a and b illustrate the linear response between the magnitude of cathodic peak (I_{pc}) and the square root of the scan rate ($v^{1/2}$). This plot linearity is evidence of a mass transport limited process on both the Au and GC electrodes. For a reversible system, the Randles–Sevcik

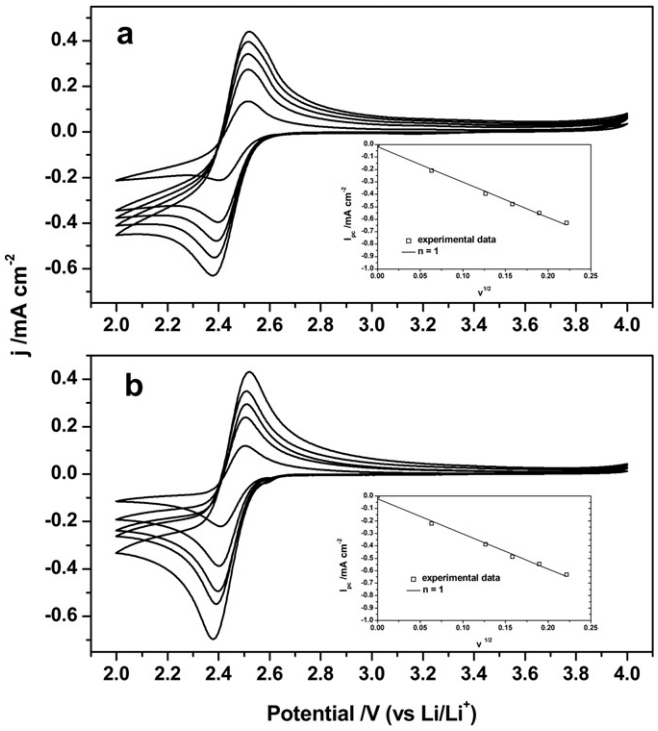

Fig. 1. CVs on the (a) Au and (b) GC electrode in 0.1 M $TBAClO_4$/NMP at various scan rates (scan rates are 49 mV s^{-1}, 36 mV s^{-1}, 25 mV s^{-1}, 16 mV s^{-1}, 4 mV s^{-1}). The insets show the Randles–Sevick plot for the cathodic peak currents, including the experimental data along with one electron theoretical fit.

equation (Eq. (1)) is used to quantify the electron transfer during the oxygen reduction. According to Eq. (1),

$$I_{pc} = 2.69 \times 10^5 n^{3/2} A D^{1/2} C v^{1/2} \quad (1)$$

where I_{pc} is a function of number of electrons transferred (n), A is the electrode area (cm^2), D is the O_2 diffusion coefficient (cm^2 s^{-1}), C is concentration of electroactive species (mol/L) and v is the scan rate (V s^{-1}). D is calculated from the Stokes–Einstein equation (Eq. (2)), which describes the relationship between the diffusion coefficient and viscosity. In Eq. (2),

$$D = kT/(6\pi\eta a) \quad (2)$$

where a is the effective hydrodynamic radius of O_2 and is substituted by the O_2 bond length of 121 pm [5], η is viscosity of NMP and the value is 1.65 mpa s and k and T are the Boltzmann constant and temperature, respectively. Using all of the values mentioned above in Eq. (2), we obtain the D value of 1.09×10^{-5} cm^2 s^{-1}. The magnitude of the O_2 diffusion coefficient in $TBAClO_4$/NMP is in good agreement with the values for that in other aprotic organic electrolytes [5,24]. C is obtained from the Bunsen coefficient for the single NMP solvent, and the value is 3.2×10^{-3} mol L^{-1}.

Comparing the experimental data and the theoretical plots, the results show that the experimental data are in close agreement with the n=1 plot, thereby indicating that the ORR in $TBAClO_4$/NMP is a one-electron transfer process; therefore, the redox couple is $O_2/O_2^{\bullet-}$. This behaviour is identical to previous work and could be explained using the Pearson's hard-soft acid base (HSAB) theory that the soft acid TBA^+ could stabilize the soft base $O_2^{\bullet-}$. In the presence of quaternary ammonium, the formation of superoxide resulting from the oxygen electroreduction and the high reversibility of $O_2/O_2^{\bullet-}$ is indicative of the chemical stability of the NMP solvent molecules with superoxide radical [4]. The increased stability of NMP could be attributed to that the energy barrier is so high (exceeds 40 kcal mol^{-1}) that nucleophilic attack at any ring carbon atom is forbidden during the oxygen reduction process [4].

Fig. 2 illustrates the O_2 reduction reaction on the Au and GC electrodes in 0.1 M $LiClO_4$/PC and 0.1 M $LiClO_4$/NMP. The CVs for 0.1 M $LiClO_4$/PC present a single cathodic peak (E_{pc1} = ~2.2 V) on the Au and GC electrodes. The anodic peaks decrease to one order of magnitude lower than that of the cathodic peak and could hardly be observed. This irreversible electrochemical profile is strongly indicative of the poor chemical stability of carbonate solvent molecules in the presence of superoxide radical, which has been confirmed by extensive research works. In contrast, the CVs for 0.1 M $LiClO_4$/NMP demonstrate two obvious oxidation peaks following a single reduction peak, and the onset potentials are similar on both Au and GC electrodes. A single cathodic peak that results in two anodic peaks suggests that the oxygen reduction in NMP is accompanied by chemical reactions. This profile is similar to that of some other aprotic electrolytes, such as ionic liquids and acetonitrile, and indicates that the reduction process is irreversible [21,25]. The accumulation of adsorbates (such as products from chemical reactions) on the GC electrode surface signifies the differences between the shapes of cathodic peaks on Au and GC electrodes. These differences in peak shape are also indicative of a different transfer coefficient, α [21]. The potentials of the two anodic peaks on the Au electrodes are approximately 3.2 V (E_{pa1}) and 3.4 V (E_{pa2}). We notice that both of these two peaks are positively shifted on the GC electrode and are not evidently separated. These observations suggest different behaviours of the electrochemical processes on different types of electrodes. A more detailed analysis of the ORRs and OERs in Li^+-containing electrolytes is proposed below.

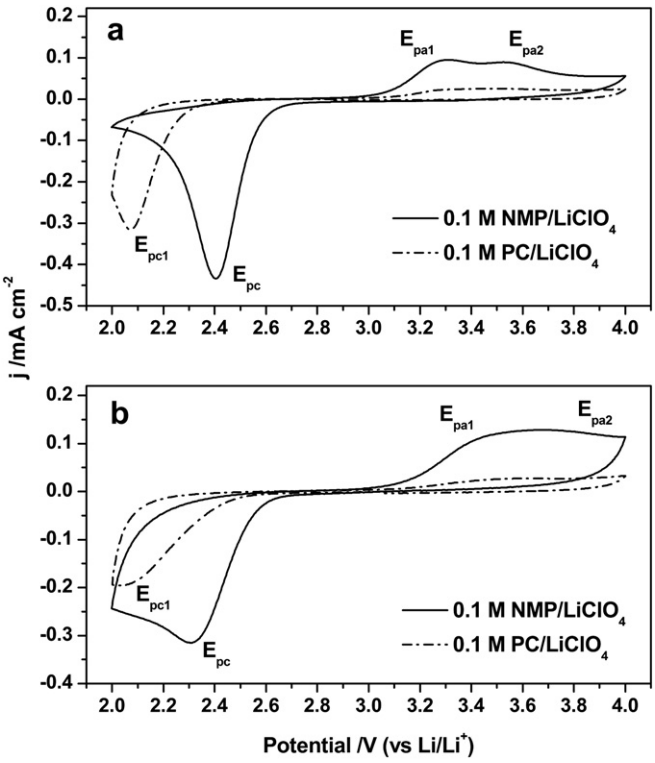

Fig. 2. CVs on the (a) Au and (b) GC electrode in 0.1 M $LiClO_4$/NMP and 0.1 M $LiClO_4$/PC at scan rate of 49 mV s^{-1}.

In an attempt to quantify the electron transfer during the irreversible oxygen reduction in the presence of Li salts, the CVs on the Au and GC electrodes in a 0.1 M $LiClO_4$/NMP electrolyte at various scan rates are presented in Fig. 3. Cathodic peak shifting to a further negative position with an increase of the scan rate also suggests that the ORR on both electrodes in $LiClO_4$/NMP electrolyte is an irreversible process. The linear response between the magnitude of I_{pc} and the square root of scan rate (inset graphs) also indicates that the irreversible reaction is a diffusion-controlled process. Because the Randles–Sevcik equation cannot be applied to irreversible systems, the Nicholson–Shain relationship (Eq. (3)), which is developed for irreversible electrochemical reactions, is used to analyse the CVs:

$$I_{pc} = 2.99 \times 10^5 n(n\alpha)^{1/2} A D^{1/2} C v^{1/2} \quad (3)$$

Here, the symbols in Eq. (3) have their usual meanings, as mentioned above. α is the transfer coefficient. Assuming a low concentration of salt does not have great effect on the diffusion coefficient and the dissolved concentration of O_2 in electrolyte; we use the D and C values from the Randles–Sevcik equation above to calculate the theoretical plot.

As observed in insets of Fig. 3, the theoretical n=1 plot can be fit to the experimental data when α=0.41 and 0.21 for the CVs on the Au and GC electrodes, respectively. Given that the reduction is irreversible, the value of α is reasonable. The different values for the transfer coefficient on the Au and GC electrodes are also consistent with the explanation of the difference between the shapes of cathodic peak. According to the fitting results, it can be concluded that oxygen reduction in the presence of Li salt is a one-electron transfer reaction and that LiO_2 is likely the predominant product. However, as expected from HSAB theory because of the high charge density, the acidity of Li^+ is significantly stronger than TBA^+; therefore, LiO_2 shows very poor stability and some of the LiO_2 decomposes into Li_2O_2 through a chemical disproportionation reaction. LiO_2 disproportioning to Li_2O_2 is responsible for the feature in the CVs, where a single cathodic peak is followed by two anodic peaks.

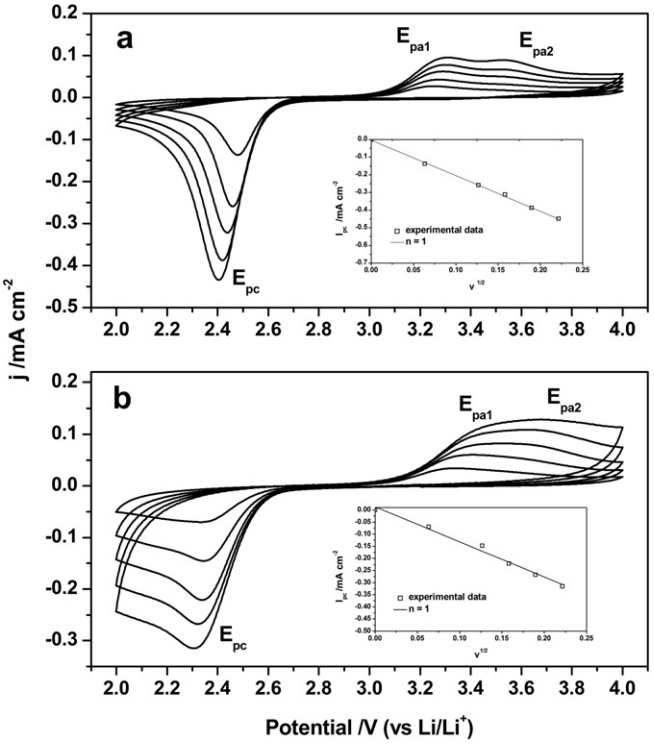

Fig. 3. CVs on the (a) Au and (b) GC electrode in 0.1 M $LiClO_4$/NMP at various scan rates (scan rates are 49 mV s^{-1}, 36 mV s^{-1}, 25 mV s^{-1}, 16 mV s^{-1}, 4 mV s^{-1}). The insets show the Nicholson–Shain plot for the cathodic peak currents, including the experimental data along with one electron theoretical fit.

Another significant observation from the scan rate dependence of the oxygen electrochemical reactions on Au and GC electrodes is that, with the increasing of scan rate, the second anodic peak (E_{pa2}) is gradually spilt from the first peak (E_{pa1}). This common feature on the two types of electrodes suggests that the OERs in $LiClO_4$/NMP contain two electrochemical reactions. These two electrochemical reactions share nearly the same standard potential, and the electron transfer in the second reaction is somewhat slower. Hence, at low scan rate, both of these reactions endure enough time at the same potential where the reactions could occur; therefore, only one anodic peak could be observed. In contrast, as the applied potential on the electrodes quickly shifts to a further positive position at a much higher scan rate, the residual reactants of the slower second electrochemical reaction would generate a comparatively obvious current at a higher overpotential and the anodic wave is split. According to the kinetic characteristics of these two electrochemical reactions, the first anodic peak (E_{pa1}) is attributed to the oxidation of LiO_2, which is believed that the kinetic of this process is rapid [23], and the second anodic peak (E_{pa2}) is assigned to the oxidation of Li_2O_2.

Comparing the current ratio of E_{pa1}/E_{pa2}, the ratio is higher on the Au electrodes than on GC. This result could be attributed to the fact that the Au atoms may stabilize LiO_2 more effectively than GC, by sustaining more LiO_2 after the ORRs and resulting in a more evident oxidation current of LiO_2 [21]. In addition to this result, when the scan rate is increased, the anodic peaks on the Au electrodes remain centred at a similar position, whereas the peaks for GC shift to a more positive position. This observation is indicative of the catalytic role that Au atoms play during the oxidation process. The catalytic effect of Au could also be confirmed by the current changes on the different electrodes after several cycles in the CVs. As observed in Fig. 4, little loss in the cathodic peak current after three cycles demonstrates good "reversible" performance of the oxygen electrochemical reactions on the Au electrode. However, the cathodic peak current rapidly diminishes during these cycles, which is indicative of the passivation caused by the accumulation of reduction products on the GC electrode surface.

Fig. 5a demonstrates the specific capacities of cells taking 0.1 M $LiClO_4$/NMP as an electrolyte at various current densities. The specific capacity is 2250 mAh g^{-1} and the average discharge voltage is about 2.6 V at a current density of 0.1 mA cm^{-2}. At higher current densities of 0.2, 0.3 and 0.5 mA cm^{-2}, the discharge voltage reduces and capacities decreased rapidly with increasing current density. The rate capability of cells taking NMP based electrolyte could be explained by the fact that oxygen reduction in Li-air batteries is a diffusion-controlled process. Fig. 5b shows the voltage–capacity curves for the above cells at a current density of 0.1 mA cm^{-2}. The average charge voltage is approximately 3.8 V during the first cycle. This charge profile is similar to that of pure Li_2O_2 electrodes. We noticed that the charge voltage of the pure carbon air electrode is lower than that in the batteries, which use carbonate-based electrolytes; even the electrodes are loaded with some catalyst [26,27]. The first cycle discharge specific capacity is 2250 mAh g^{-1}, and the charge specific capacity is 2180 mAh g^{-1}. The efficiency is approximately 97% during the first cycle, and the cell demonstrates good cyclic performance. During the second and third recharging, the charge plateau rises to approximately 4.0 V and completely disappears during the last two cycles. As observed in Fig. 5c, when cycling between 2.0 V and 4.1 V for several cycles, the discharge

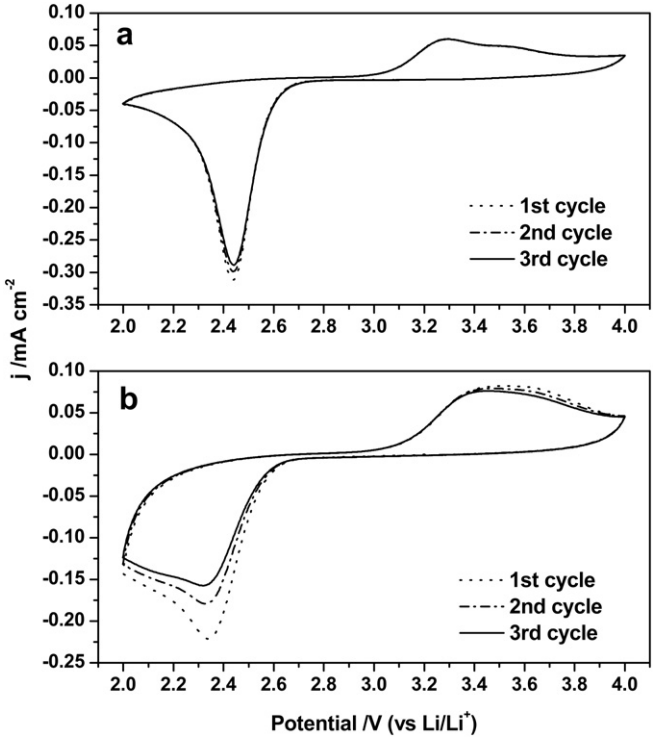

Fig. 4. CVs on the (a) Au and (b) GC electrode in 0.1 M $LiClO_4$/NMP at scan rate of 25 mV s^{-1} with three cycles.

capacity and the efficiency gradually decrease. After five cycles, the discharge capacity decreases to only 475 mAh g^{-1}, and the efficiency is approximately 75%.

Fig. 6 shows the Raman spectra of the electrodes in different steps of the cycles for the purpose of studying the reason for performance deterioration. Each other Raman spectrum is collected on two different spots to give more comprehensive information of deposits on the surface of electrodes at different stages. The Raman spectrum of the as-prepared electrode (Fig. 6a) presents two characteristic peak of carbon. After the first discharge, peaks at 818 cm^{-1} and 204 cm^{-1} in the Raman spectrum (Fig. 6b) are attributed to the vibrations of the O—O bond and Li—O bond [18,25]. These peaks suggest that the discharge products are Li_2O_2. The Raman spectrum of the electrode after the first charge (Fig. 6c) reflects the disappearance of the vibration of O—O bond and a weaker intensity of the peak that is attributed to the vibration of Li—O bond. This result indicates that most of the Li_2O_2 decomposed during the charge process. The peak at 1040 cm^{-1}, which could be assigned to the vibration of CO_3^{2-}, indicates the formation of Li_2CO_3 [18] during the recharge. After five cycles, as observed in Fig. 6d, characteristic peaks of Li_2CO_3 and Li—O bond become more evident. Besides these two obvious characteristic peaks, a weak peak indicating of the vibration of O—O bond could also be observed. The reappearance of characteristic peak of O—O bond could be attributed to the accumulation of undecomposed Li_2O_2 on the surface of electrodes during cycle. This observation shows that deposits on the electrode surface after five cycles mainly contain Li_2CO_3 and undecomposed Li_2O_2.

For further investigation of the changes in the composition of products on the electrode surface, X-ray photoemission spectra are obtained. Fig. 7 shows the wide scan survey of the electrodes surface in different steps during the cycling. Comparing this survey with the survey of the as-prepared electrode (Fig. 7a), the O 1s photoemission peak is clearly observed in the survey of electrode

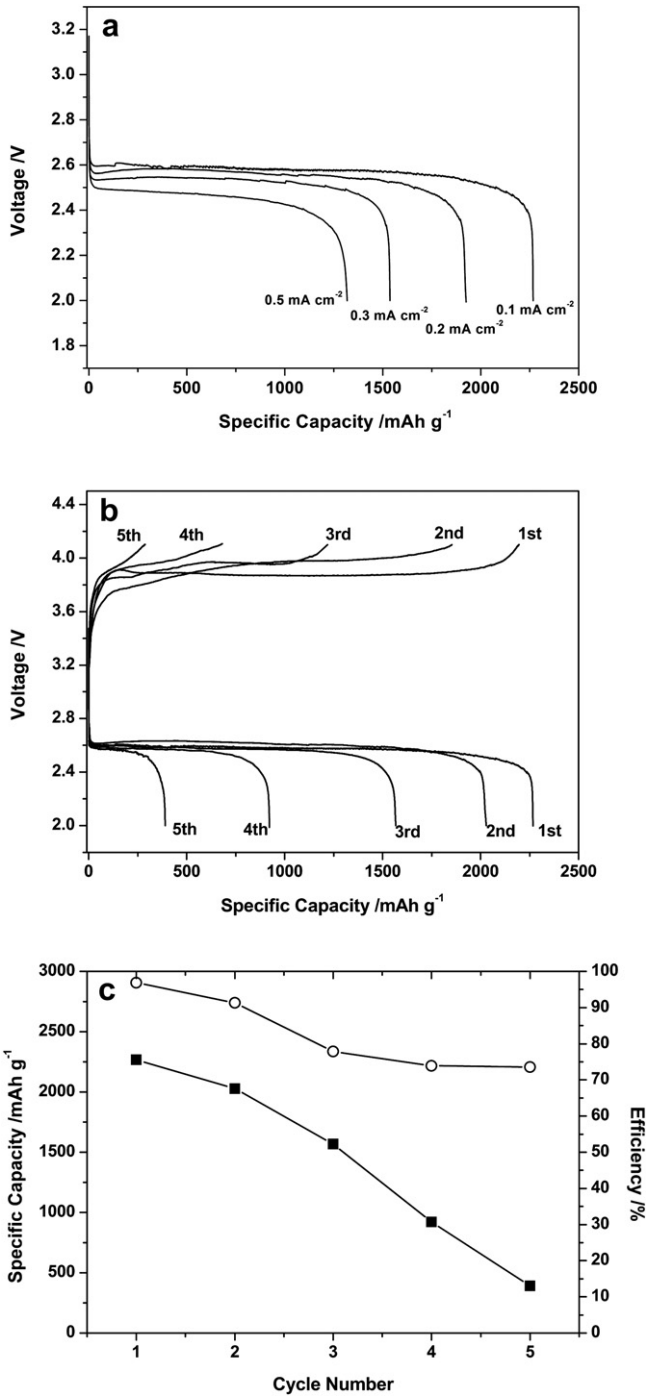

Fig. 5. (a) Voltage–capacity curves for the Li-air cells with 0.1 M $LiClO_4$/NMP as electrolyte, cycled at 0.1 mA cm^{-2} between 2.0 V and 4.1 V. (b) Variation of discharge capacity and efficiency with cycle number.

after the first discharge (Fig. 7b). The amount of surface oxygen-containing products is observed to decrease after the first charge, as indicated by the decreasing intensity of the O 1s peak. Although the O 1s peak intensity is decreased, the evident differences in the intensity of the O 1s peak between the surveys of electrode as-prepared and after the first charge suggests that there is a certain amount of oxygen-containing compounds (Li_2O_2 and Li_2CO_3) that deposit onto the electrode surface (see in Fig. 6c). Furthermore, a weak N 1s peak is observed in the survey of the electrode after the first charge, and this peak becomes somewhat stronger after five

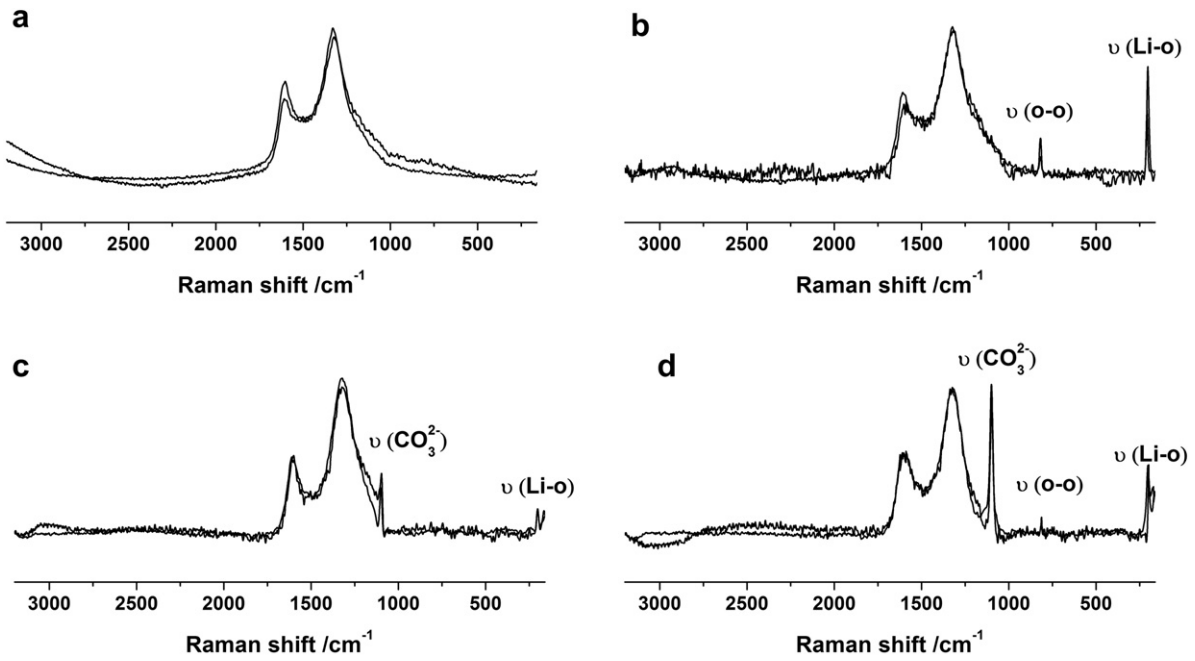

Fig. 6. Raman spectra of the electrodes at different steps in cycling (a) as-prepared (b) after first discharge (c) after first charge (d) after five cycles.

cycles. Because this peak is not observed in the survey of the as-prepared electrode, which provides evidence that the as-prepared electrode does not contain N, the appearance of N 1s peak could only be attributed to the decomposition of solvent during the charge process.

Fig. 8 illustrates the elemental analysis from XPS. All of the deconvoluted peaks are labelled by the corresponding structure. An XPS analysis of the C 1s spectra shows a detailed change on the electrode surface. After the first discharge, the C 1s spectra is fitted to three peaks, which are attributed to sp^2 hybridized graphite-like carbons (284.8 eV), sp^3 hybridized diamond-like carbons (285.6 ± 0.1 eV) and >C═O bond (286.8 ± 0.1 eV) [28]. The binding energies of these peaks do not change greatly during cycling. The main change in the C 1s spectra of the electrode after the first charge is the appearance of a peak at 289.4 eV, which is attributed to the formation of Li_2CO_3. Stronger intensity of this peak in the C 1s spectra of cycled electrode suggests the increased amount of Li_2CO_3 that deposits onto the electrode surface. This result is in agreement with the Raman spectroscopy. Further analysis of O 1s and Li 1s spectra of electrodes demonstrate that after the first discharge, the discharge product is Li_2O_2 (56.1 ± 0.1 eV in Li 1s spectra and 532.9 eV in O 1s spectra) [29,30]. When the first charge process is completed, deposits on the electrode surface contain Li_2CO_3 (55.1 eV in Li 1s spectra and 531.4 ± 0.1 eV in O 1s spectra) and trace amount of undecomposed Li_2O_2. These two compounds also exist on the surface of electrode after five cycles (Fig. 8c). In addition to these two compounds, though the content is much smaller compared to Li_2CO_3, we observed that the peak that is indicative of $LiNO_x$ could be deconvoluted from the O 1s and Li 1s spectra (55.3 eV in Li 1s spectra and 532.3 eV in O 1s spectra) of the electrodes after the first charge; this peak becomes somewhat more evident after five cycles. The peak where the binding energy is 399.8 eV in the N 1s spectra of these electrodes also provides evidence of the existence of $LiNO_x$. The appearance of peaks that are indicative of the formation of Li_2CO_3 and $LiNO_x$ suggests that NMP may decompose under an O_2 atmosphere during the recharging. These products passivate the surface of the electrode and lead to the elevation of the charge plateau during the second and third recharging (as observed in Fig. 5b).

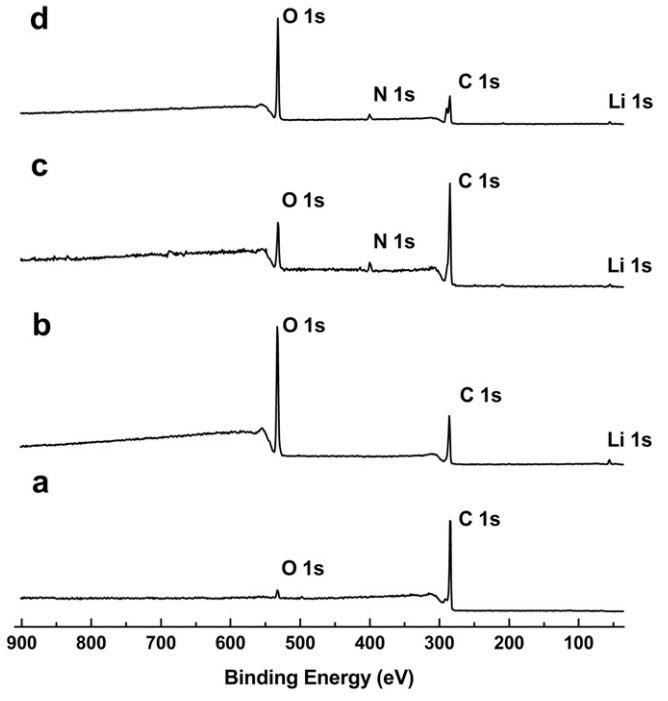

Fig. 7. XPS wide scan survey of the electrodes at different steps in cycling (a) prepared (b) after first discharge (c) after first charge (d) after five cycles.

According to Figs. 6–8, the main products of cells taking NMP as electrolyte after first discharge is Li_2O_2. This result also demonstrates the increased stability of NMP during discharge. However, obvious decomposition of NMP is observed on the actual air electrodes. This result could be attributed to the porosity of Super P that is quite different from the compact GC electrodes. As shown in Fig. 9, the diameters of these mesoporous on actual air electrodes

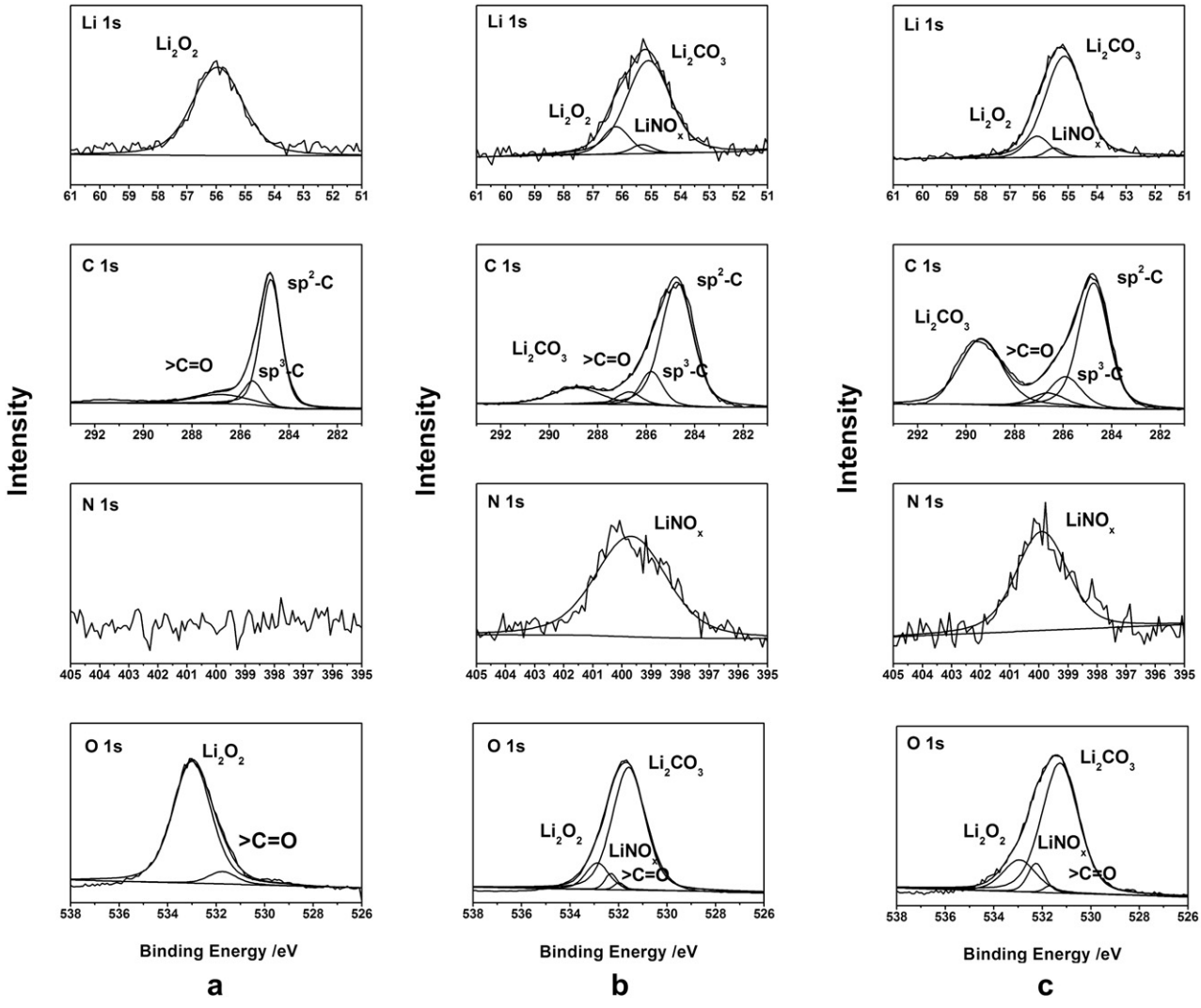

Fig. 8. Li 1s, C 1s, N 1s and O 1s spectra of the electrodes at different steps in cycling (a) after first discharge (b) after first charge (c) after five cycles.

mainly distributes in the range of 3∼5 nm. These mesoporous have high surface energy and could promote the decomposition of NMP. To demonstrate the various electrochemical behaviours on the two different carbon electrodes, Fig. 10 shows the CVs on the GC and the actual air electrodes employing either F105 or PVDF as binders. Comparing the CVs on GC, the cathodic peaks shift to a more

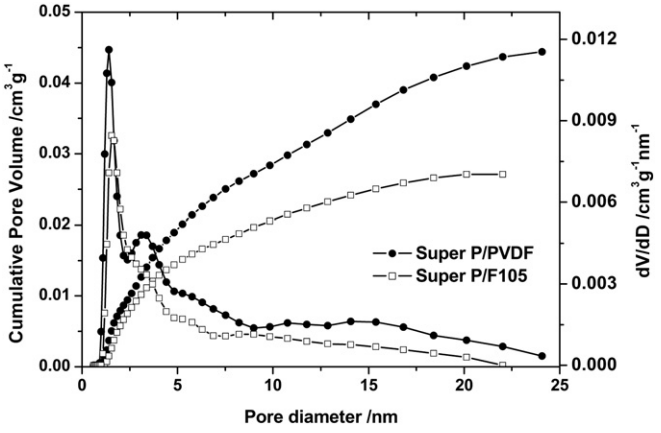

Fig. 9. Cumulative pore volume and pore size distribution of actual air electrodes using various pointers.

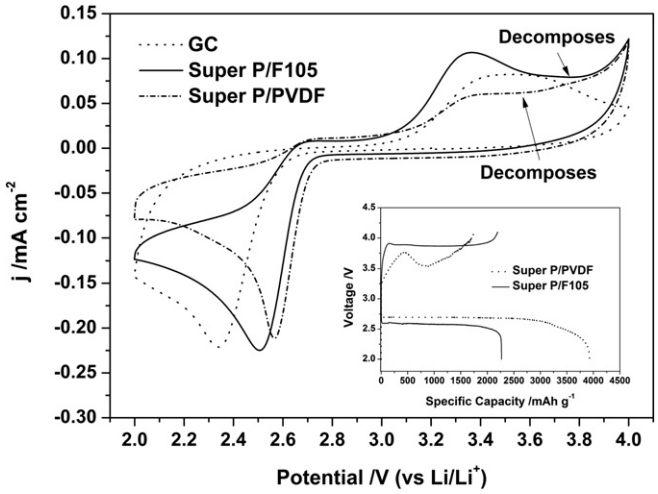

Fig. 10. (a) CVs on the GC and air electrodes with either F105 or PVDF as binders at 25 mV s^{-1}. (b) Voltage–capacity curves for Li-air cells with cathodes employing either F105 or PVDF as binders at 0.1 mA cm^{-2} between 2.0 V and 4.1 V.

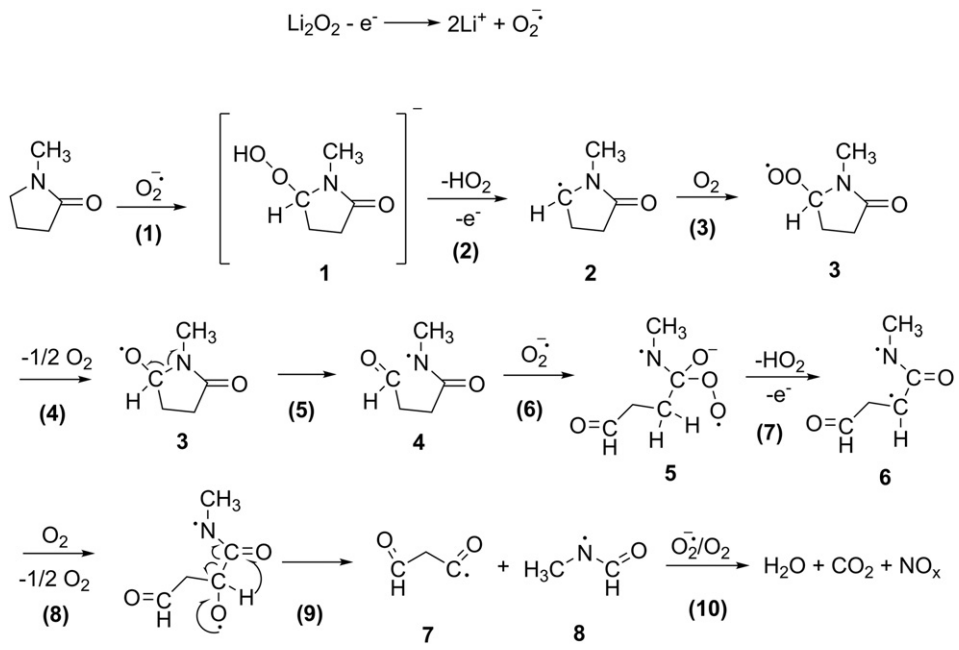

Scheme 1. Proposed mechanism for decomposition of NMP during discharge.

positive position on both of the actual air electrodes, which indicate a faster oxygen reduction process on Super P than on the GC. The result could also be attributed to the mesoporous on Super P. Another evident distinction is that the decomposition currents of the electrolyte are observed in the CVs for both of the actual air electrodes. We believed that the binders do not cause such obvious decomposition currents because of their small content in the working electrode. Elemental analysis of XPS (see above) also supports this conclusion. The decomposition potential of NMP on the Super P/F105 air electrode is about 3.8 V. This value indicates that NMP has already begun to decompose during the first recharge and that, as the charge voltage increases to approximately 4 V during the following two cycles, the decomposition of solvent becomes more drastic and results in the degradation of performance. On the other hand, the decomposition of NMP occurs at more negative potential (~3.5 V) on the Super P/PVDF air electrode, and peaks indicative of the oxidation of the oxygen reduction species disappear. Consequently, as observed in the inset in Fig. 10, the cells using Super P/PVDF as cathodes demonstrate no charge plateau, even during the first cycling.

The above results suggest that porosity of carbon materials that are used to prepare air cathodes is the fundamental reason for the decomposition of NMP. However, because binders could change the mesoporous distribution and pore volume [31], selection of binders is also very important to the performance of cells. According to Fig. 9, Super P/PVDF is larger in pore volume and pore distribution ranged from 3 to 5 nm than that of Super P/F105. The result indicates that air electrodes employing PVDF as binders could provide more active site for oxygen reduction and NMP decomposition than that taking F105 as binders. Hence, the specific capacity and discharge plateau of Super P/PVDF is higher than Super P/F105. Simultaneously, during charge process, decomposition of NMP becomes more rapidly on Super P/PVDF. Therefore, the more negative decomposition potential and disappearance of charge plateau are observed on the actual air electrodes taking PVDF as binders, which are shown in Fig. 10.

A mechanism for the electrolyte decomposition is shown in Scheme 1. The decomposition of NMP during charge process could be attributed to the preferential attack by superoxide ion at the ring CH_2 group adjacent to the nitrogen atom [32]. As a result of the high reactivity of mesoporous on Super P and the electrochemical oxidation during charge process, this reaction could occur at ambient conditions. Commencing with Li_2O_2 oxidation to $O_2^{\bullet-}$, $O_2^{\bullet-}$ can attack the ring CH_2, reaction 1, to form 5-Hydroperoxo-1-methyl-2-pyrrolidione (intermediate 1) [32]. By removing HO_2 [33] and electrochemical oxidation, reaction 2, intermediate 1 form carbon radical (intermediate 2). Reaction with O_2 molecule, carbon radical yield peroxo radical (intermediate 3) which proceeds to the alkoxy radical (intermediate 4) [33]. In the presence of alkoxy radical, homolytic cleavage occur at C—N bond [34] and the 5-membered lactam opens to form a straight-chain alkyl amides (intermediate 4). Because intimidate 4 is a straight-chain alkyl amides, carbonyl group of intermediate 4 could be attacked by $O_2^{\bullet-}$ [33], yielding a 5-membered cyclic transition state (intermediate 5) to form a carbon radical (intermediate 6), reaction 7. Similar with reactions 3 and 4, the resulting carbon-centered radical reacts with O_2 to form intermediate 7 which decomposes to two new radicals (intermediate 7 and 8) via a homolytic cleavage reaction. Followed by oxidative decomposition, these radicals result in formation of H_2O, CO_2 and NO_x [33,35,36]. Generated H_2O, CO_2 and NO_x further react with Li_2O_2 to form Li_2CO_3 and $LiNO_x$ which are detected on the surface of the air electrodes.

4. Conclusions

In conclusion, although the presence of Li salt strongly influences the behaviour of the ORRs and OERs, the basic electrochemical reaction is a one-electron transfer process that generates $O_2/O_2^{\bullet-}$ couples. Because of the stronger acidity of Li^+, the initially formed LiO_2 disproportionates to the predominant discharge product Li_2O_2. During recharge, Li_2O_2 could decompose at a high overpotential and Au atoms would catalyse the oxidation of Li_2O_2, with evidence of no passivation on the gold electrode surface by multiple cycles. Other than the above reactions, no other chemical reactions, such as nucleophilic reactions between $O_2^{\bullet-}$ and solvent molecules, are observed in the NMP-based electrolyte. The increased chemical stability of NMP against oxygen reduction species results in the good performances of the NMP-based cells. In addition, for the further application of NMP-based electrolytes in rechargeable Li-air batteries with high cyclic performance, it is

very important that preventing the decomposition of NMP on the surface of porous air electrodes.

References

[1] G. Girishkumar, B. McCloskey, A.C. Luntz, S. Swanson, W. Wilcke, The Journal of Physical Chemistry Letters 1 (2010) 2193–2203.
[2] A. Kraytsberg, Y. Ein-Eli, Journal of Power Sources 196 (2011) 886–893.
[3] R. Padbury, X. Zhang, Journal of Power Sources 196 (2011) 4436–4444.
[4] V.S. Bryantsev, V. Giordani, W. Walker, M. Blanco, S. Zecevic, K. Sasaki, J. Uddin, D. Addison, G.V. Chase, The Journal of Physical Chemistry A 115 (2011) 12399–12409.
[5] J. Read, K. Mutolo, W.B.M. Ervin, J. Wolfenstine, A. Driedger, D. Foster, Journal of the Electrochemical Society 150 (2003) A1351–A1356.
[6] W. Xu, J. Xiao, D. Wang, J. Zhang, J.-G. Zhang, Journal of the Electrochemical Society 157 (2010) A219–A224.
[7] W. Xu, J. Xiao, J. Zhang, D. Wang, J.-G. Zhang, Journal of the Electrochemical Society 156 (2009) A773–A779.
[8] S.S. Zhang, K. Xu, J. Read, Journal of Power Sources 196 (2011) 3906–3910.
[9] V.S. Bryantsev, M. Blanco, The Journal of Physical Chemistry Letters 2 (2011) 379–383.
[10] S.A. Freunberger, Y. Chen, Z. Peng, J.M. Griffin, L.J. Hardwick, F. Barde, P. Novak, P.G. Bruce, Journal of the American Chemical Society 133 (2011) 8040–8047.
[11] J. Xiao, J. Hu, D. Wang, D. Hu, W. Xu, G.L. Graff, Z. Nie, J. Liu, J.-G. Zhang, Journal of Power Sources 196 (2011) 5674–5678.
[12] W. Xu, K. Xu, V.V. Viswanathan, S.A. Towne, J.S. Hardy, J. Xiao, Z. Nie, D. Hu, D. Wang, J.-G. Zhang, Journal of Power Sources 196 (2011) 9631–9639.
[13] W. Xu, V.V. Viswanathan, D. Wang, S.A. Towne, J. Xiao, Z. Nie, D. Hu, J.-G. Zhang, Journal of Power Sources 196 (2011) 3894–3899.
[14] B.D. McCloskey, D.S. Bethune, R.M. Shelby, G. Girishkumar, A.C. Luntz, The Journal of Physical Chemistry Letters 2 (2011) 1161–1166.
[15] J. Read, Journal of the Electrochemical Society 153 (2006) A96–A100.
[16] S.A. Freunberger, Y. Chen, N.E. Drewett, L.J. Hardwick, F. Bardé, P.G. Bruce, Angewandte Chemie International Edition 50 (2011) 8609–8613.
[17] C.O. Laoire, S. Mukerjee, E.J. Plichta, M.A. Hendrickson, K.M. Abrahama, Journal of the Electrochemical Society 158 (2011) A302–A308.
[18] H. Wang, K. Xie, Electrochimica Acta 64 (2012) 29–34.
[19] Z. Zhang, J. Lu, R.S. Assary, P. Du, H.-H. Wang, Y.-K. Sun, Y. Qin, K.C. Lau, J. Greeley, P.C. Redfern, H. Iddir, L.A. Curtiss, K. Amine, The Journal of Physical Chemistry C 115 (2011) 25535–25542.
[20] T. Kuboki, T. Okuyama, T. Ohsaki, N. Takami, Journal of Power Sources 146 (2005) 766–769.
[21] C.J. Allen, S. Mukerjee, E.J. Plichta, M.A. Hendrickson, K.M. Abraham, The Journal of Physical Chemistry Letters 2 (2011) 2420–2424.
[22] K. Izutsu, Electrochemistry in Nonaqueous Solutions, Wiley-VCH, Weinheim, 2009.
[23] C.O. Laoire, S. Mukerjee, K.M. Abraham, The Journal of Physical Chemistry C 113 (2009) 20127–20134.
[24] C.O. Laoire, S. Mukerjee, K.M. Abraham, E.J. Plichta, M.A. Hendrickson, E.J. Plichta, M.A. Hendrickson, The Journal of Physical Chemistry C 114 (2010) 9178–9186.
[25] Z. Peng, S.A. Freunberger, L.J. Hardwick, Y. Chen, V. Giordani, F. Bardé, P. Novák, D. Graham, J.M. Tarascon, P.G. Bruce, Angewandte Chemie International Edition 50 (2011) 6351–6355.
[26] H. Cheng, K. Scott, Journal of Power Sources 195 (2010) 1370–1374.
[27] A. Debart, A.J. Paterson, J. Bao, P.G. Bruce, Angewandte Chemie International Edition 47 (2008) 4521–4524.
[28] S.W. Lee, B.-S. Kim, S. Chen, Y. Shao-Horn, P.T. Hammond, Journal of the American Chemical Society 131 (2009) 671–679.
[29] D. Ensling, A. Thissen, W. Jaegermann, Applied Surface Science 255 (2008) 2517–2523.
[30] Q.-H. Wu, A. Thissen, W. Jaegermann, Applied Surface Science 250 (2005) 57–62.
[31] S.R. Younesi, S. Urbonaite, F. Björefors, K. Edström, Journal of Power Sources 196 (2011) 9835–9838.
[32] R.S. Drago, R. Riley, Journal of the American Chemical Society 112 (1990) 215–218.
[33] Y. Chen, S.A. Freunberger, Z. Peng, F. Barde, P.G. Bruce, J of the American Chemical Society 134 (2012) 7952–7957.
[34] A. Miller, P.H. Solomon, Writing Reaction Mechanisms in Organic Chemistry second ed., Academic Press, San Diego, California, USA, 1999.
[35] R. Atkinson, International Journal of Chemical Kinetics 29 (1997) 99–111.
[36] A. Sinha, M.J. Thomson, Combustion and Flame 136 (2004) 548–556.